71

SATELLITE & MESOMETEOROLOGY
RESEARCH PROJECT

Department of the Geophysical Sciences
The University of Chicago

A STUDY OF MESOSCALE CLOUD MOTIONS COMPUTED FROM ATS-I AND TERRESTRIAL PHOTOGRAPHS

by

Tetsuya Fujita and Dorothy L. Bradbury
The University of Chicago

and

Clifford Murino and Louis Hull
St. Louis University

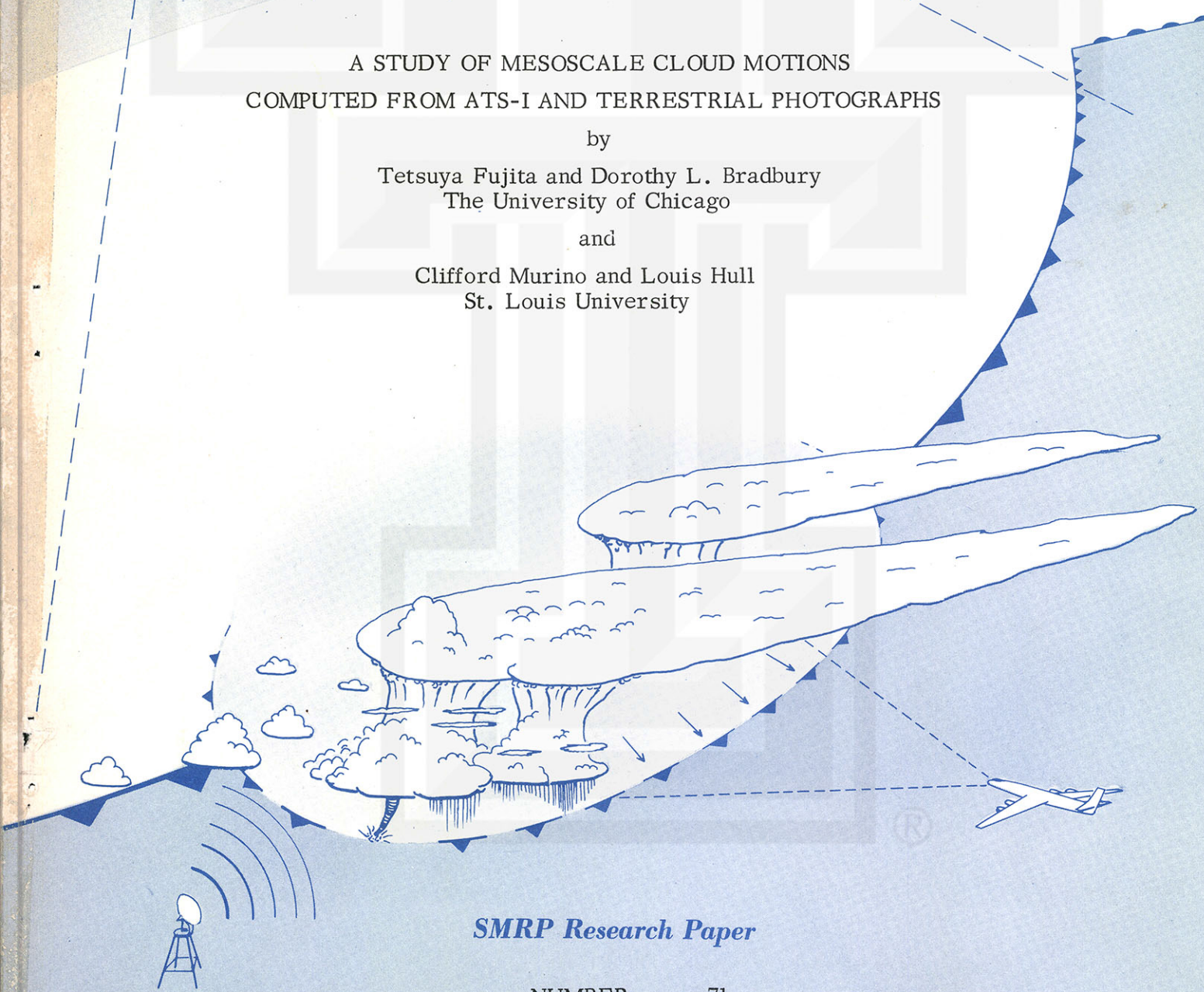

SMRP Research Paper

NUMBER 71

March 1968

MESOMETEOROLOGY PROJECT --- RESEARCH PAPERS

1.* Report on the Chicago Tornado of March 4, 1961 - Rodger A. Brown and Tetsuya Fujita

2.* Index to the NSSP Surface Network - Tetsuya Fujita

3.* Outline of a Technique for Precise Rectification of Satellite Cloud Photographs - Tetsuya Fujita

4.* Horizontal Structure of Mountain Winds - Henry A. Brown

5.* An Investigation of Developmental Processes of the Wake Depression Through Excess Pressure Analysis of Nocturnal Showers - Joseph L. Goldman

6.* Precipitation in the 1960 Flagstaff Mesometeorological Network - Kenneth A. Styber

7.** On a Method of Single- and Dual-Image Photogrammetry of Panoramic Aerial Photographs - Tetsuya Fujita

8. A Review of Researches on Analytical Mesometeorology - Tetsuya Fujita

9. Meteorological Interpretations of Convective Nephsystems Appearing in TIROS Cloud Photographs - Tetsuya Fujita, Toshimitsu Ushijima, William A. Hass, and George T. Dellert, Jr.

10. Study of the Development of Prefrontal Squall-Systems Using NSSP Network Data - Joseph L. Goldman

11. Analysis of Selected Aircraft Data from NSSP Operation, 1962 - Tetsuya Fujita

12. Study of a Long Condensation Trail Photographed by TIROS I - Toshimitsu Ushijima

13. A Technique for Precise Analysis of Satellite Data; Volume I - Photogrammetry (Published as MSL Report No. 14) - Tetsuya Fujita

14. Investigation of a Summer Jet Stream Using TIROS and Aerological Data - Kozo Ninomiya

15. Outline of a Theory and Examples for Precise Analysis of Satellite Radiation Data - Tetsuya Fujita

16. Preliminary Result of Analysis of the Cumulonimbus Cloud of April 21, 1961 - Tetsuya Fujita and James Arnold

17. A Technique for Precise Analysis of Satellite Photographs - Tetsuya Fujita

18. Evaluation of Limb Darkening from TIROS III Radiation Data - S.H.H. Larsen, Tetsuya Fujita, and W.L. Fletcher

19. Synoptic Interpretation of TIROS III Measurements of Infrared Radiation - Finn Pedersen and Tetsuya Fujita

20. TIROS III Measurements of Terrestrial Radiation and Reflected and Scattered Solar Radiation - S.H.H. Larsen, Tetsuya Fujita, and W.L. Fletcher

21. On the Low-level Structure of a Squall Line - Henry A. Brown

22. Thunderstorms and the Low-level Jet - William D. Bonner

23. The Mesoanalysis of an Organized Convective System - Henry A. Brown

24. Preliminary Radar and Photogrammetric Study of the Illinois Tornadoes of April 17 and 22, 1963 - Joseph L. Goldman and Tetsuya Fujita

25. Use of TIROS Pictures for Studies of the Internal Structure of Tropical Storms - Tetsuya Fujita with Rectified Pictures from TIROS I Orbit 125, R/O 128 - Toshimitsu Ushijima

26. An Experiment in the Determination of Geostrophic and Isallobaric Winds from NSSP Pressure Data - William Bonner

27. Proposed Mechanism of Hook Echo Formation - Tetsuya Fujita with a Preliminary Mesosynoptic Analysis of Tornado Cyclone Case of May 26, 1963 - Tetsuya Fujita and Robbi Stuhmer

28. The Decaying Stage of Hurricane Anna of July 1961 as Portrayed by TIROS Cloud Photographs and Infrared Radiation from the Top of the Storm - Tetsuya Fujita and James Arnold

29. A Technique for Precise Analysis of Satellite Data, Volume II - Radiation Analysis, Section 6. Fixed-Position Scanning - Tetsuya Fujita

30. Evaluation of Errors in the Graphical Rectification of Satellite Photographs - Tetsuya Fujita

31. Tables of Scan Nadir and Horizontal Angles - William D. Bonner

32. A Simplified Grid Technique for Determining Scan Lines Generated by the TIROS Scanning Radiometer - James E. Arnold

33. A Study of Cumulus Clouds over the Flagstaff Research Network with the Use of U-2 Photographs - Dorothy L. Bradbury and Tetsuya Fujita

34. The Scanning Printer and Its Application to Detailed Analysis of Satellite Radiation Data - Tetsuya Fujita

35. Synoptic Study of Cold Air Outbreak over the Mediterranean using Satellite Photographs and Radiation Data - Aasmund Rabbe and Tetsuya Fujita

36. Accurate Calibration of Doppler Winds for their use in the Computation of Mesoscale Wind Fields - Tetsuya Fujita

37. Proposed Operation of Intrumented Aircraft for Research on Moisture Fronts and Wake Depressions - Tetsuya Fujita and Dorothy L. Bradbury

38. Statistical and Kinematical Properties of the Low-level Jet Stream - William D. Bonner

39. The Illinois Tornadoes of 17 and 22 April 1963 - Joseph L. Goldman

40. Resolution of the Nimbus High Resolution Infrared Radiometer - Tetsuya Fujita and William R. Bandeen

41. On the Determination of the Exchange Coefficients in Convective Clouds - Rodger A. Brown

* Out of Print
** To be published

(Continued on back cover)

SATELLITE AND MESOMETEOROLOGY RESEARCH PROJECT
Department of the Geophysical Sciences
The University of Chicago

A STUDY OF MESOSCALE CLOUD MOTIONS COMPUTED FROM ATS-I AND TERRESTRIAL PHOTOGRAPHS

by

Tetsuya Fujita and Dorothy L. Bradbury
The University of Chicago

and

Clifford Murino and Louis Hull
St. Louis University

SMRP Research Paper No. 71

March 1968

The research reported in this paper has been sponsored by the Meteorological Satellite Laboratory, ESSA, under Grant Cwb WBG-34 and the National Science Foundation under Grants No. GA-864 and GA-410.

A STUDY OF MESOSCALE CLOUD MOTIONS COMPUTED FROM ATS-I AND TERRESTRIAL PHOTOGRAPHS[1. 2.]

by

Tetsuya Fujita and Dorothy L. Bradbury
The University of Chicago

and

Clifford Murino and Louis Hull
St. Louis University

1. Introduction

In conjunction with the Line Island Experiment operating near the subsatellite point of ATS-I, a terrestrial camera network was established by The University of Chicago and St. Louis University at the top of Haleakala volcano on Maui, Hawaii. The purpose of the operation was to identify and interpret the cloud elements appearing in a series of ATS-I pictures taken at 23-min intervals.

Meanwhile, several methods for determining the velocities of clouds from ATS picture sequences efficiently were explored at the Satellite and Mesometeorology Research Project, The University of Chicago, leading to the construction of a loop projector.

As a result, it is now feasible to compare cloud velocities computed independently from satellite and ground photogrammetry. Since the computation of cloud velocities from ATS pictures is carried out exclusively by filming ATS pictures in various modes, the computation method may be identified as the "cinegrammetric method" of cloud-velocity computation.

2. ATS-I Cloud Pictures in Relation to Upper-Air Flow over the North Pacific

In order to describe the large-scale cloud patterns over the central North Pacific, an ATS-I picture taken between 1354 and 1414 HST 15 March 1967 was gridded with 10-deg longitude and latitude intervals (see Fig. 1). Hawaii is situated to the southeast of a well-developed cyclone centered near 35N 170W. A long, anvil-like plume emanating

---

1. The research reported in this paper has been sponsored by the Meteorological Satellite Laboratory, ESSA, under Grant Cwb WBG-34 and the National Science Foundation under Grants No. GA-864 and GA-410.

2. This paper is scheduled to appear in ATS-I Volume, University of Wisconsin.

from a large cellular cloud was passing over Hawaii, giving the impression that the plume was embedded in a strong jet stream passing over the island.

Both the 300- and 500-mb charts at 1400 HST on 15 March 1967 were analyzed as shown in Fig. 2. It is seen that a well-developed low to the northwest of Hawaii appears on the 500-mb chart as a very small, closed circulation which did not extend to 300 mb. A blocking high, somewhat like that defined by Rex (1950), extended far to the north of Hawaii near 160W. The southern branch of the jet stream, split by the blocking high, extended from north of Hawaii toward the west coast of the United States. At 300 mb, the maximum wind speed along the jet axis was over 100 kt. At the 500-mb level the wind maximum was located between Hawaii and 120W. West of the blocking high, a jet stream was seen over Japan on both the 300- and 500-mb charts.

When these jet-stream patterns are compared closely with the ATS-I picture in Fig. 1, which was taken within 10 min of the 1400 HST map time, it will be found that there appears to be no jet-stream cirrus in the area of the jet stream extending eastward from Japan. Even a time-lapse movie made from an ATS-I picture sequence did not show any fast-moving, high clouds over the expected jet position. The ATS-I picture clearly shows a long plume-like band of clouds extending east-northeast from about 10N 175W to California, passing over Hawaii. Significant motion of cloud elements within this long band can be seen on an ATS-I time-lapse movie. The movie also shows that plumes from the tops of convective cells far to the south of the band converge toward the band, indicating confluent flow toward the area of the jet stream at 500 mb. The single frame ATS-I picture in Fig. 1 indicates such a confluent pattern made visible by the orientation of faint plumes.

The equatorial zone was generally cloud free, while the northern ITC was characterized by scattered convective cells with horizontal dimensions of up to about 300 km.

3. Computation of Cloud Motions from ATS Pictures using the SMRP Loop Projector

After viewing a large number of time-lapse movies of ATS-I pictures, the authors became convinced that they are extremely useful in gaining knowledge of the development and motion of clouds. In many cases, the difference in the direction of cloud motions permits us to distinguish those clouds located at different levels. Three different

directions of cloud motion were observed within a small area, suggesting that they could be used in determining the vertical distribution of winds if we could relate cloud and wind velocities.

In order to determine the cloud velocities on a movie screen it is necessary to follow a specific cloud element or cloud mass as it travels for a short distance during its life time or for the period of the daylight hours, whichever is shorter. Usually, the cloud life is much shorter than 12 hr, the average daylight period in lower latitudes. By filming two frames of every picture taken at 23-min intervals, changes in cloud during a 10 hr period, for instance, will be shown in about 60 frames and it appears on a movie screen in about three seconds. A cloud with a one- to two-hour lifetime would appear on only about 8 to 14 frames, which would not exceed one second of projection time.

In an attempt to prolong the projection time of specific cloud elements with about a one-hour lifetime, a cyclic filming technique was explored. This involves selecting a series of about five pictures and then filming them according to the schedule described in Table I.

Table I. An example of cyclic filming to produce various modes of reciprocal motion of a cloud. In this case, a series of five pictures, identified as numbers 1 through 5, were filmed in three filming modes.

Picture Number	1	2	3	4	5	4	3	2
Oscillation Mode	(16)	(3)	(3)	(3)	(16)	(3)	(3)	(3)
Quick-return Mode	(16)	(3)	(3)	(3)	(16)	(1)	(1)	(1)
Instant-return Mode	(16)	(3)	(3)	(3)	(16)	(0)	(0)	(0)

A cyclic filming in the oscillation mode is done by exposing picture No. 1 sixteen times, pictures No. 2, 3, and 4 three times each, picture No. 5 sixteen times; then by making three exposures each of No. 4, 3, and 2 to complete the first cycle consisting of 50 frames. In order to produce a 250-frame endless loop, for instance, five such cycles should be completed. When such a loop is projected at 16 frames sec^{-1}, the

clouds on the first frame remain on the screen for one second; then they move very fast, taking only a fraction of a second, toward their positions on the fifth picture, which is shown for one second. Thereafter all clouds return to their positions on the first frame, taking only about half a second.

Shown in Fig. 3 is the loop projector designed and constructed at the Satellite and Mesometeorology Research Project (SMRP) at the University of Chicago. The loop projector takes a film loop with a total of between 200 and 300 frames. Such a loop may be projected for hours using a 500-watt bulb without damage to the film. The image is focused on the outer surface of a rectangular transparent glass plate with a 45 deg tilt. A sheet of tracing paper is taped on the outer surface of the glass and cloud motions are traced directly on the paper. To avoid the bending of the loop film because of the heat a push switch has been disigned to turn on both the lamp and the fan simultaneously, but it will turn off only the lamp. The fan is shut off automatically by a pre-set timer after the projector cools. The film loop continues to run with the projection light off.

When a film loop is made in the quick-return mode, clouds stay in their positions on the first and fifth pictures for one second each. Unlike the oscillation-mode case, clouds move slowly from the first to the fifth picture, then they quickly return to their initial positions. In this mode, therefore, an analyst can tell immediately the direction of the cloud movement, which is more readily observed than in the oscillation mode.

By returning from the fifth to the first picture instantaneously, we produce a film in the instant-return mode. The projected image shows that all clouds simply move from the first to the fifth picture positions in repeated fashion . It was found that a film in this mode is also very useful in obtaining quickly a field of cloud velocities.

There are a large number of other filming modes that can be used for various purposes. We have also tested a three-color mode in thich the first and fifth pictures are tinted in red and blue respectively, while the second, third, and fourth pictures remain black. It was found, however, that a rapid change in color within a short time does not create a comfortable feeling for our eyes. The use of identical color for all frames and the adoption of various filming modes seem to satisfy most of the necessities for the computation of cloud velocities with our loop projector.

We shall now discuss the continuity of cloud images appearing on successive ATS pictures taken at 23-min intervals. In order to identify easily the change in shape and

position of the clouds on each picture, a set of six pictures, representing identical sections from enlarged prints, was pasted together in Fig. 4. The 8×10 inch negatives showing the global view used for making these prints were furnished by Prof. Suomi of the University of Wisconsin. The picture start time in Hawaiian Standard Time is indicated near the lower left corner of each picture.

As shown in the 1549 HST picture, the direction of the scan is very close to the east-west direction. The five major islands of Hawaii are indicated by arrows pointing toward the mostly cloud-covered islands. The largest and highest island, Hawaii, appears in all the pictures as a large white area with an elongated hole near the western edge of the cloud-covered area. This hole represents that part of the island above the top of the clouds including Mauna Loa and Mauna Kea.

The large convective cloud west of Hawaii shows some rotational characteristics. The rotation center is apparent in the pictures for 1526 and 1549 HST and was located near the west end of the cloud mass with horizontal dimensions of about 200 km. A long plume of middle cloud extended eastward from the large convective cloud and passed over the islands of Maui and Hawaii practically the entire day.

In order to make a test analysis of the cloud motion in the vicinity of Hawaii, an area shown in Fig. 5 was selected from the ATS-I picture, for which scanning started at 1223 HST. The area of individual clouds is out lined by thin lines inside of which the areas of bright clouds are stippled. As indicated in the figure, some 200 points were selected in order to determine their displacement on the image plane of the loop projector. Five pictures, with scan starting times of 1223, 1246, 1309, 1332, and 1354 HST, were filmed in the quick-return mode defined in Table I. The film thus produced was projected continuously until the cloud velocities shown in Fig. 6 were obtained. These velocity vectors were then grouped together into low, middle, and unknown cloud motions which were plotted, respectively, with solid arrows, shafts and barbs, and open arrows. These cloud heights are, more or less, the speculated heights except for those over the island of Maui where a ground network of cameras was operated. Despite the fact that the ATS-I pictures do not tell us the cloud height, the patterns of cloud motion give definite indication of the differences in the cloud height when the clouds move in different directions and at different speeds from one another. The grouping of clouds in Fig. 6 into low, middle, and unknown was made tentatively, according to their movement only.

4. Photogrammetric Determination of Cloud Motion from Whole-Sky and Panoramic Pictures from Maui, Hawaii

The Satellite and Mesometeorology Research Project of the University of Chicago and St. Louis University established a camera network of stations atop the northern rim of Mr. Haleakala on Maui during the early part of March 1967, and it was in operation from 13 March through 3 April. The purpose of the network was to gather photographic cloud data during the period of the Line Island Experiment and the ATS-I picture acquisition in order to study the time changes in mesoscale nephsystems and to compute the motions of clouds in the region of the Hawaiian Islands. A comparison was made between the values of cloud motions determined in this manner and those computed from ATS-I pictures using the SMRP loop projector described in the previous section.

Three different camera systems were used to gather the photographic data, namely, whole-sky cameras, panoramic cameras, and stationary wide-angle movie cameras. The whole-sky cameras were set to take 16-mm color movies at intervals of 20 sec during the daylight hours, and the wide-angle time-lapse movie cameras were set to take 16-mm time-lapse movies at 15-sec intervals during daylight hours. The panoramic cameras were manually operated 35-mm cameras using IR film and were equipped with 35-mm lenses. Eight consecutive pictures were taken, each centered on an octant beginning with N, then NE, etc. This allowed about a 7-deg overlap of the coverage of adjacent frames. Panoramic pictures were taken at 20-min intervals and as near as possible to the ATS picture acquisition schedule.

Figure 7 shows the photographic network established at three sites on Mt. Haleakala. The two wide-angle time-lapse cameras were mounted on the roof of a building at the Kolekole site (elevation of about 9990 ft) with one camera pointing toward the island of Hawaii and the other toward the island of Lanai. At the Red Hill site (elevation 10,010 ft), a whole-sky and a panoramic camera were placed about 25 ft apart and were designated "Station A". At 3.6 km north-northeast of this station, the second whole-sky camera station was erected at the Kalahaku site, or "Station B". In order to get the best available view in all octants, the panoramic IR stand was erected on a peak approximately 0.3 km south-southwest of the whole-sky site.

A stereo-pair of the whole-sky pictures is shown in Fig. 8. It was impossible to have the two cameras synchronized perfectly, but two pictures taken within a few

seconds of each other are acceptable as a stereo-pair. Selecting such a pair was accomplished by making a plot of frame number vs. time for each camera and then choosing the frames most closely simultaneous. A large number of detached clouds or cloud elements can be identified on each picture of the stereo pair. Only six from a large number of clouds chosen from these two pictures used for computation of height and motion are labeled.

Before cloud height and cloud motion can be computed, the whole-sky parabolic mirrors must first be calibrated in order to determine the horizon and elevation angles. This can be done by different techniques. One method is to compute the angles theoretically by using the dimensions of the parabola. This assumes that the mirrors are perfect and that the principal point was exactly at the center of the circular image. The most practical method was to select a picture-taking day when the sky had been mostly clear and to plot a composite of the sun's images during the day. Then using the Fujita technique and a Transverse Equidistant Cylindrical Projection overlay (1963) the zenith angles of the solar image, ζ , were determined. Labeling the parallels as $(90 - \zeta)$, the elevation angles of cloud images could then be read.

The distance of a specific cloud or cloud element is determined by the intersection of the azimuth-angle rays from the two cameras at a known base-line distance apart. Figure 9 shows a result of determining the position and height of six different clouds, numbered 1 to 6, which are indicated in the picture in Fig. 8. The heights of these clouds were determined by using the computed distances and the elevation angles. Table II shows the examples of various parameters thus obtained. The computed cloud motions were determined from consecutive images taken within a one-minute interval. These values agree quite well with the wind-speed values reported from Kahalui and Hilo at the 5- to 6-km level at 1400 HST, as well as with the values of cloud motion computed on the loop projector. The values computed from the loop projector were average motions of larger cloud masses for a period of approximately 90 minutes. More details on computation techniques are described by Bradbury and Fujita (1967).

Since infrared more or less penetrates atmospheric haze, clouds with tops at 5 km could be photographed up to about 440 km from the station. Shown in Fig. 10 are an enlarged view of the ATS-I picture started at 1526 HST (top), and the three sections of the panoramic view taken at 1520 HST. As can be seen in both pictures, the only

Table II. Computed range of clouds from whole-sky camera stations, their height (MSL) and cloud motion for clouds shown in the stereo-pair of Fig. 8. Cloud motion was computed as a 1-min average. Clouds numbered 1 to 6 are shown in Fig. 8.

Cloud No.	Distance from A (km)	Distance from B (km)	Elev. ∠ A (deg)	Elev. ∠ B (deg)	Height A (km)	Height B (km)	Mean Cloud Motion (kt)
1	17.0	13.5	8.5	11.0	5.5	5.5	
2	7.1	5.0	21.0	30.0	5.7	5.7	
3	7.1	6.6	19.0	20.0	5.4	5.3	31.9
4	5.1	6.6	24.0	19.4	5.2	5.2	38.4
5	5.9	9.1	27.2	17.0	5.9	5.7	45.3
6	8.4	7.7	19.5	24.4	6.0	6.3	57.4
7	11.3	8.2	10.0	15.0	5.0	5.0	
8	11.4	8.8	12.0	16.3	5.4	5.4	
9	7.4	5.1	18.0	25.0	5.4	5.2	
10	9.9	7.8	8.5	11.0	4.5	4.4	
11	10.0	8.4	7.5	10.7	4.3	4.4	
12	9.6	8.1	7.2	11.2	4.2	4.4	
13	6.6	5.3	20.0	25.3	5.4	5.3	
14	5.0	4.7	28.0	29.7	5.6	5.5	
15	3.6	4.7	34.3	29.0	5.5	5.5	
16	7.4	7.9	16.8	16.5	5.2	5.2	33.5
17	7.8	8.9	17.0	13.7	5.3	5.0	39.9
18	10.3	11.5	11.3	11.0	5.1	5.1	39.9
19	7.3	9.0	18.0	15.0	5.4	5.2	
20	4.0	6.4	29.5	20.0	5.3	5.2	
21	3.4	6.2	29.8	20.0	5.0	5.1	31.9
22	5.9	8.3	20.0	15.2	5.2	5.1	
23	6.8	10.0	13.5	10.2	4.7	4.7	31.9
24	3.6	7.1	20.0	13.0	4.3	4.5	
25	2.2	5.6	39.0	20.0	4.8	4.9	
26	22.3	22.2	10.0	10.0	6.9	6.8	
27	5.4	5.8	25.4	27.8	5.6	5.9	50.0
28	8.0	9.2	20.0	19.0	5.9	5.9	

clouds in the northerly direction are those surrounding the island of Maui at low elevations. They do not reach to the height of the camera station. To the northeast, at a range of about 100 km, two cloud lines can be observed on the ATS photograph. With the use of the nomogram shown in Fig. 11, the intersection of the 100-km distance line with the zero elevation angle would give a 0.75-km height, indicating that these are probably low cumuli. To the southwest of Maui in the ATS-I picture, a line of clouds extending toward the island can be observed. These can be identified in the SW panoramic view as the line of altocumulus passing directly over the station. In the southeasterly direction, the top of Mauna Loa and Mauna Kea can be seen protruding above the top of the low-level stratocumulus. The area between Maui and Hawaii appears to be cloud-free on the ATS-I photograph as well as on the panoramic view. But a W-E line of clouds about 75 km south of Maui on the ATS-I picture appears as a line about 3 deg above the horizon on the panoramic view (middle strip). Using Fig. 11, this would give a cloud height of approximately 5 km, which agrees with the cloud height computed for those clouds from the same streamer passing over Maui. Any number of such cloud masses within a 400 km range from Maui can easily be matched with those appearing on the ATS-I picture providing there is nothing obstructing the view. Thus, if the range can be determined from the ATS-I view and elevation angle from the panoramic view, the cloud height is easily computed.

5. Analysis of Soundings

Photogrammetric determination of cloud heights and velocities in Section 4 revealed that the plume-like clouds that extended from a large convective cloud west of Hawaii were mostly of the altocumulus type with heights ranging between about 4.5 and 6.5 km MSL. Their speed varied from 30 to 50 kt.

Since the large convective cloud was located half-way between Johnston Island and Hilo, some 1400 km apart in a WSW-ENE direction, we shall attempt a detailed analysis of the soundings at 1400 HST from these stations. As shown in Figs. 12 and 13, the atmosphere above 700 mb over Johnston Is. was very dry, suggesting that the subsidence in the subtropical high reached down to about 700 mb. On the other hand, there was a marked moist layer over Hilo between the 520- and 600-mb surfaces. The heights of these pressure surfaces correspond to the cloud heights measured by the Maui camera network. From these moisture distributions we may postulate that most

of the outflow from the convective cloud passed over Hawaii at about 5 km MSL.

Winds over Johnston Is. between the 500- and 600-mb surfaces were very light, increasing from 20 to 25 kt. Over Hilo, however, the winds at corresponding heights increased from 38 to 53 kt, indicating that the wind velocity inside the moist layer was about 45 kt from the west. It is of interest to note that the velocity of the plume-like clouds in the vicinity of Hilo was about 40 kt. This means that the motion of the altocumulus over Hawaii computed from ATS-I pictures represents the winds at the cloud level. The horizontal dimensions of the altocumulus used in the velocity computation were kept below about 50 km.

At higher levels, the wind speed increased upward, reaching a maximum of 63 kt at about 200 mb over Johnston Is. and 103 kt at 250 mb over Hilo. None of the cloud velocities computed from ATS-I pictures indicated such high velocities. Furthermore, no cirrus-type clouds drifting from the west were observed from the Maui network stations. It is therefore very likely that the top of the large convective cloud west of Hawaii was not as high as the clouds of the average midwestern thunderstorm. If the cloud top reached the 300 mb level, for instance, more plume-like cirriform clouds should have been seen over Hawaii and they should have moved at the rate of about 100 kt.

6. Synoptic Interpretation of Cloud Motion

In the preceding sections it was found that the velocities of plume-like middle clouds over Hawaii computed from both ATS-I pictures and terrestrial stereo-pictures were identical to the wind velocities at the cloud level. This would mean that these middle clouds simply drifted away from their source region. An attempt was made, therefore, to plot the cloud velocities on upper-air charts close to these cloud heights.

A sectional surface chart at 1400 HST was constructed in Fig. 14 with all available ship and land station reports. Note that the cloud covers are indicated and low clouds are separated from middle and high clouds. Both cloud types and station temperatures are shown near each station. It is seen that the large convective cloud was located ahead of an advancing cold front followed by a weak surge of cold air. The region of Hawaii and the convective cloud was under the influence of weak, easterly trade winds with their tops located between the 800- and 870-mb surfaces.

Without verifying the height of cellular clouds which are likely to be of the low cloud type, all cloud velocities obtained by tracking these cellular clouds were plotted on an 850-mb chart for 1400 HST (see Fig. 15). Of extreme interest is the velocity of the clouds to the southeast of the convective cloud, all of which are about 12 kt from the southeast. Due to the warm tropospheric temperature over Johnston Is. as compared with that over Hilo (see Fig. 13), the height of the 850-mb surface over Johnston Is. was much higher than that over Hilo. This resulted in drawing a trough or a convergence line, as shown in Fig. 15, in order to construct height contours which would fit both the cloud motions and the 850-mb height over Johnston Island. It appears that the large convective cloud under consideration was located on this convergence line.

The 850-mb chart in Fig. 15 was constructed by taking the computed low cloud velocities and the 850-mb heights and winds into consideration. The cloud motions inside the region behind the cold front northwest of Hawaii were all from the west-southwest, suggesting that the cold air was very shallow. A convergence line far to the northeast of Hawaii was characterized by a significant horizontal shear in the cloud motion. It seems that this convergence line and the weak, warm front on the surface chart are closely related. The slope of the warm frontal surface appears to be extremely small when it is computed by combining the surface and the 850-mb charts. Such a result would be realistic in view of the errors involved in the surface chart analysis and of the transient stage of the warm front formed at the tail end of a dissipating cold front.

Figure 16 is a 500-mb chart for 1400 HST, including the middle-cloud velocities computed from the ATS-I pictures taken between 1223 and 1354 HST. Although we were not able to verify the cloud types and the height of the clouds, except those over Maui, we assume that there was no variation in the height of the plume-like clouds as they drifted eastward from their source. The cloud speeds increased significantly from 22 kt, just east of the convective cloud, to 88 kt as they crossed the 148W meridian. A similar increase in the wind speed from 34 kt over the island of Kauai to 53 kt over the island of Hawaii is seen.

Isotachs at 10 kt intervals were drawn to describe the velocity field of the cloud motions. The resulting isotach pattern turned out to be very similar to that of the entrance regions of jet streams. Note that those isotachs drawn for cloud velocities fit reasonably well with the observed winds on the 500-mb surface over the Hawaiian

island area. The direction of cloud motion was used to determine the orientation of height contours, and they showed definite directional convergence toward the core region of the 500-mb jet stream.

Using the streamline and the isotach analyses at 500 mb as shown in Fig. 16, both the divergence and the relative vorticity of middle-cloud velocities were computed by reading off the direction and the speed at grid points. Figure 17 shows that most of the jet-stream region was characterized by less than 2×10^{-5} sec^{-1} divergence. The field was more or less non-divergent despite the speed increase toward the east-northeast. The direction convergence actually cancelled out the speed increase.

The relative vorticity was divided into cyclonic to the north and anticyclonic to the south by the jet axis, showing patterns very similar to those of high-level jet streams studied by Palmen and Newton (1948). The Coriolis parameter over the area of the analysis is approximately $2\Omega \sin\phi = 5.0 \times 10^{-5} sec^{-1}$. Therefore, the absolute vorticity of the cloud velocities to the south of the jet axis turned out to be slightly anticyclonic.

According to Palmen and Newton (1948), the absolute vorticity to the south of a polar jet stream is nearly zero. Riehl, Berry, and Maynard (1955) also verified this evidence by using aircraft traverse data. A negative absolute vorticity, however, was reported by Reiter (1961), suggesting the existence of anticyclonic absolute vorticity to the south of the jet axis.

The authors do not intend to justify the computed anticyclonic absolute vorticity values, since the 500-mb surface is too low to expect anticyclonic absolute vorticity. Furthermore, the cloud velocities may not represent the air motion throughout the entire region. Nonetheless, cloud velocities of such density as was utilized in computing divergence and vorticity would be of great value in estimating the field of air motion where no data are otherwise available.

7. Summary and Conclusions

Presented in this paper are the results of the computation of cloud velocities from a series of ATS-I pictures. A local area near Hawaii was selected for such computation because a stereo-camera network was operated on top of Haleakala on Maui. Independent computation of cloud velocities from terrestrial photogrammetry revealed that

the velocities of middle clouds computed from both ATS-I and terrestrial photographs are very close to each other. These cloud velocities were found to represent approximately the wind velocities at the cloud levels.

An attempt was made to improve local upper-air analyses by adding the cloud velocities on corresponding upper-air charts even though the heights of the clouds were not known accurately. It was found that cloud velocities are very useful in determining the mesoscale field of air motions which affect the cloud motions.

Also computed were the divergence and vorticity of the cloud velocities determined from ATS-I pictures. Despite the fact that it is uncertain that a group of clouds which moves with similar velocities is located at a unique height, the computed fields are found to be quite meaningful.

Through this study of cloud motions by using ATS-I and terrestrial pictures, the authors recommend that (1) it is necessary to develop an accurate and quick method for computing cloud velocities from ATS picture sequences, (2) terrestrial photogrammetric studies of cloud heights and velocities should be performed simultaneously and independently, and (3) the relationship between the air motion and the velocity of various clouds must be established through observational and theoretical studies. After solving these problems, it will become feasible to add a large number of wind velocities at several levels by computing cloud velocities from ATS pictures.

Acknowledgements:

The authors are very grateful to Professor Verner E. Suomi, who made ATS-I pictures available to the authors' study. Much credit is due Mr. Arthur Z. Loesch of the University of Chicago who assisted in establishing and operating the panoramic and time lapse movie camera stations and to Mr. William Carlson of Meteorology Research Incorporated for his services in operating the two whole-sky camera systems. This study was performed at Maui, Hawaii and at the University of Chicago.

REFERENCES

Bradbury, Dorothy L. and T. Fujita, 1967: Computation of height and velocity of clouds from dual, whole-sky, time-lapse picture sequences. Satellite and Mesometeorology Research Project Research Paper No. 70, The University of Chicago.

Fujita, T., 1963: A technique for precise analysis of satellite data; Volume I, Photogrammetry. U.S. Dept. of Commerce, Meteorological Satellite Laboratory Report No. 14, 106 pp.

Palmen, E. and C. W. Newton, 1948: A study of the mean wind and temperature distribution in the vicinity of the polar front in winter, J. Meteor. 5, 220-226.

Reiter, E. R., 1961: The detailed structure of the wind field near the jet stream. J. Meteor., 18, 9-30.

Riehl, H., F.A. Berry, and H. Maynard, 1955: Exploration of the jet stream by aircraft during the 1952-53 winter, J. Meteor. 12, 26-35.

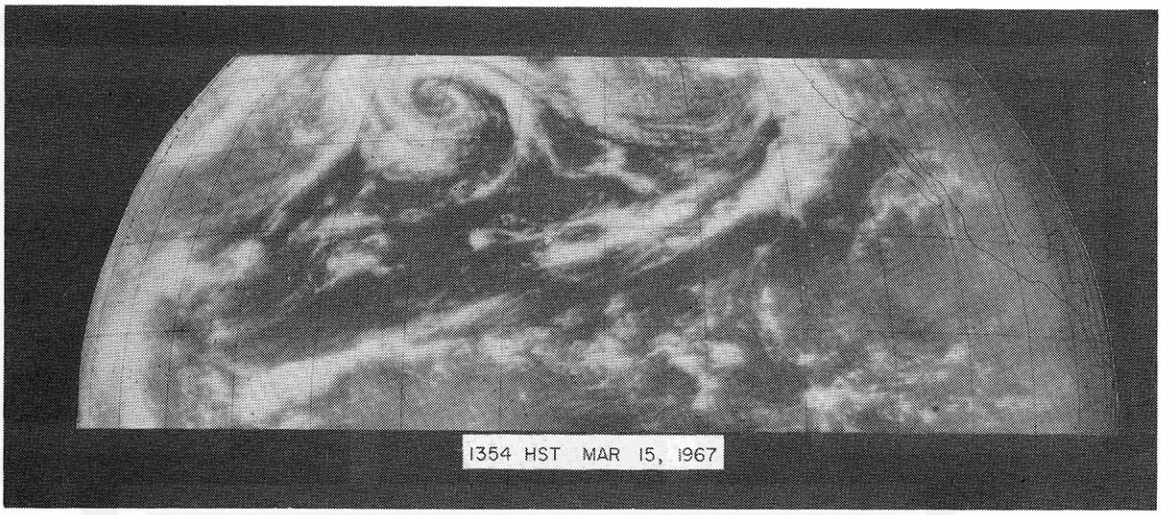

Fig. 1. An ATS-I picture started at 1354 HST 15 March 1967 showing plumes and streamers drifting eastward from a couple of large convective cloud systems. Longitudes and latitudes are drawn at 10-deg intervals.

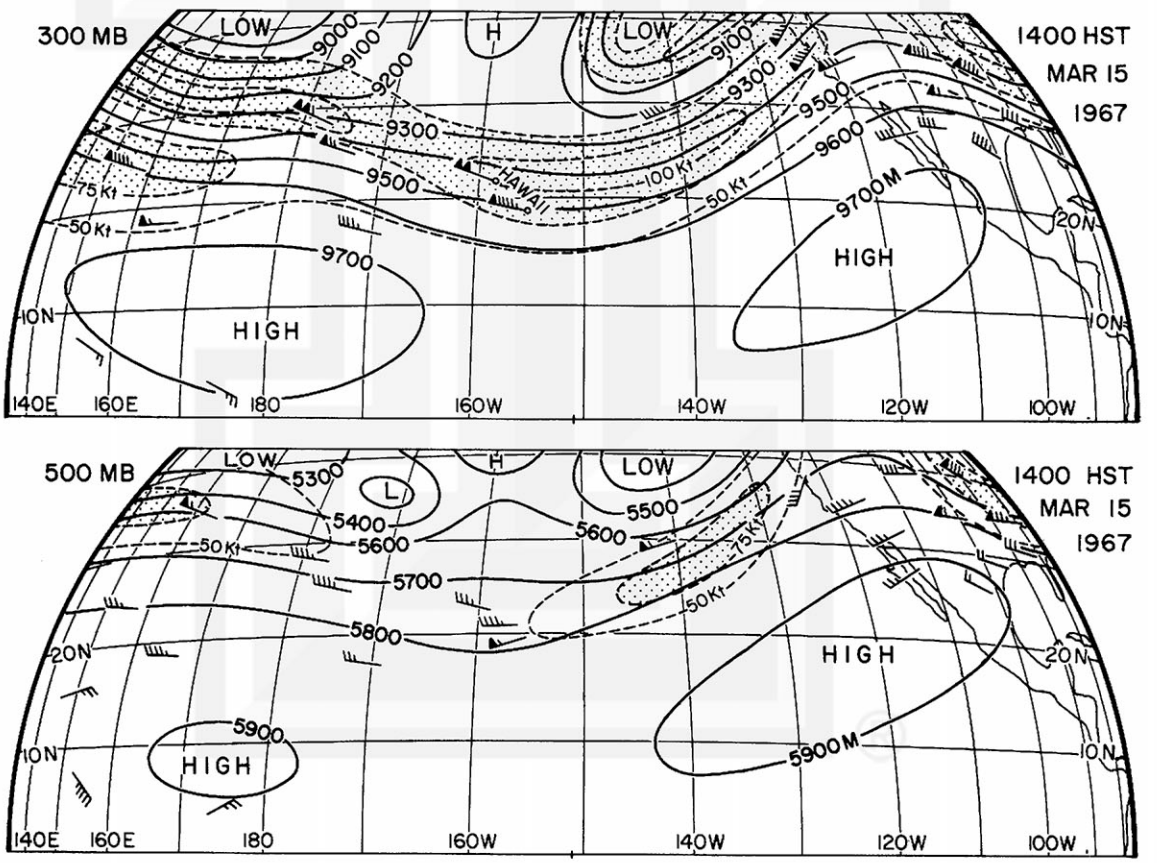

Fig. 2. Constant pressure charts at 300 and 500 mb for 1400 HST 15 March 1967. Areas with wind speed in excess of 75 kt are stippled.

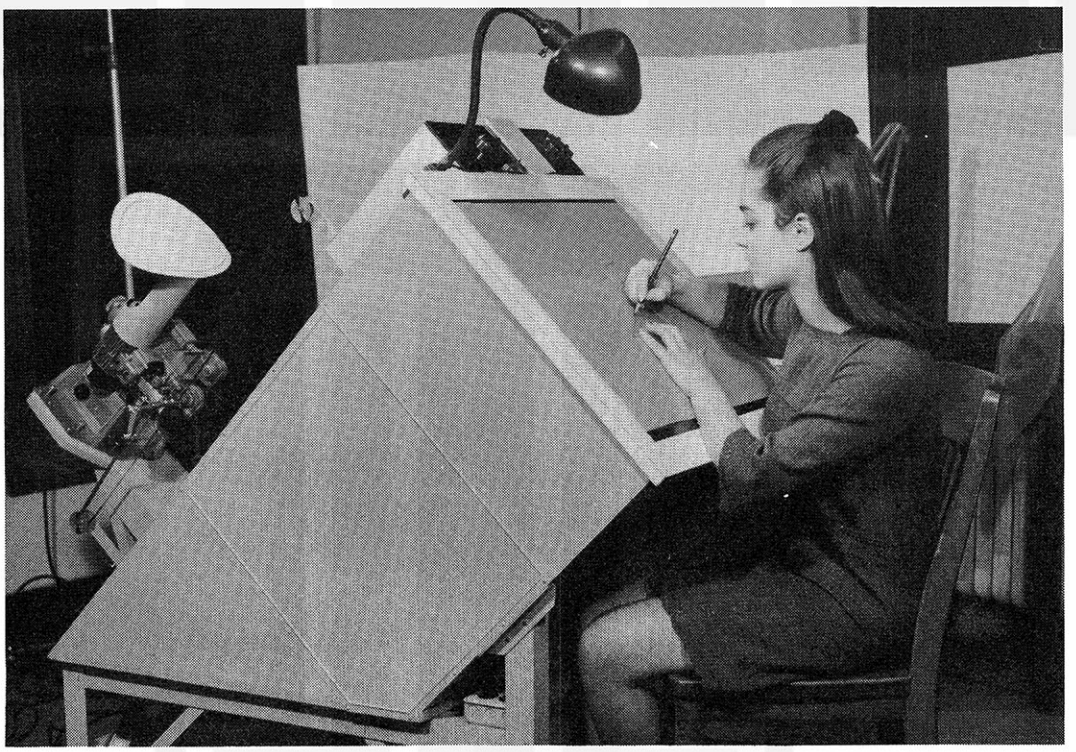

Fig. 3. A loop projector constructed by SMRP for use in cinegrammetric study of ATS cloud motions.

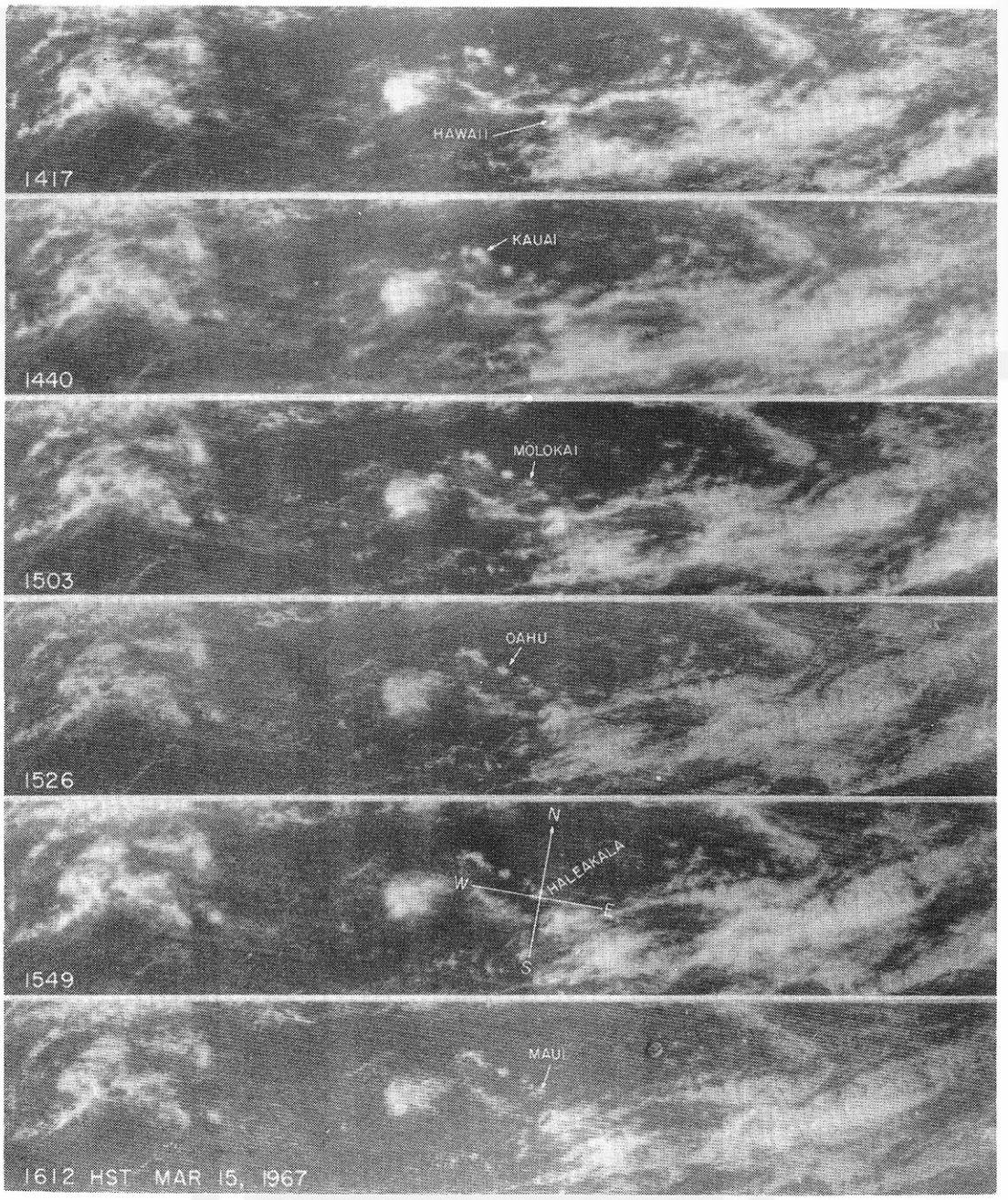

Fig. 4. A series of ATS-I pictures started at 1417, 1440, 1503, 1526, 1549, and 1612 HST 15 March 1967. These pictures were enlarged from 8 x 10 inch high-resolution negatives produced by Prof. Suomi, the University of Wisconsin.

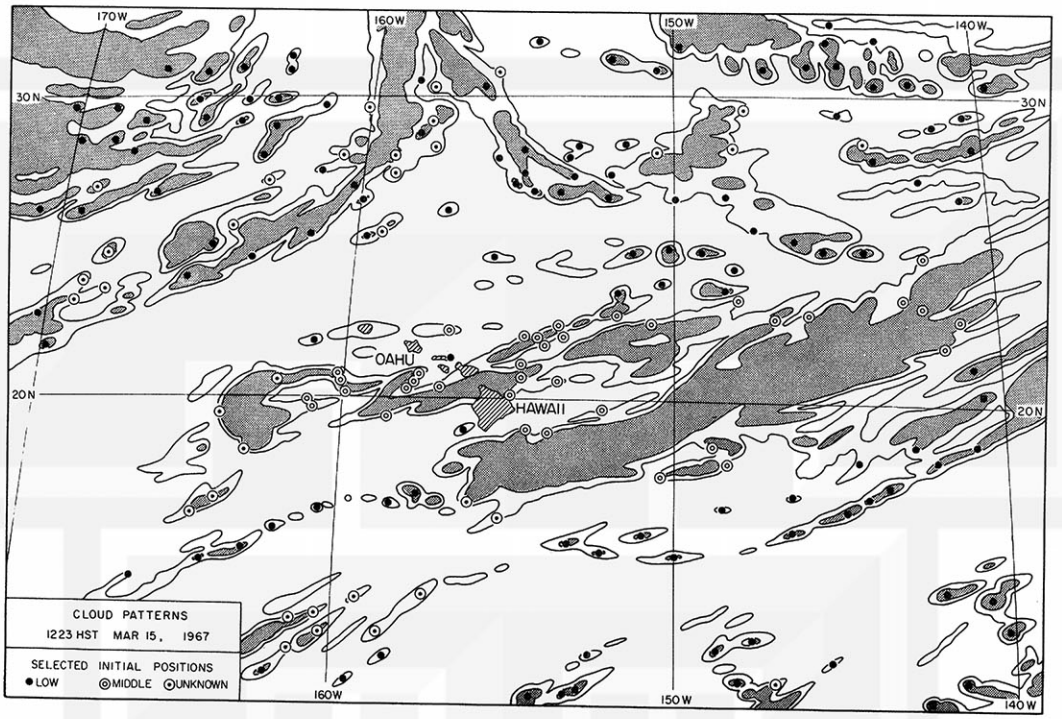

Fig. 5. Cloud patterns and cloud elements selected for computation of cloud velocities. Initial positions at 1223 HST are represented by black circles (low clouds), double circles (middle clouds), and encircled dots (unknown clouds).

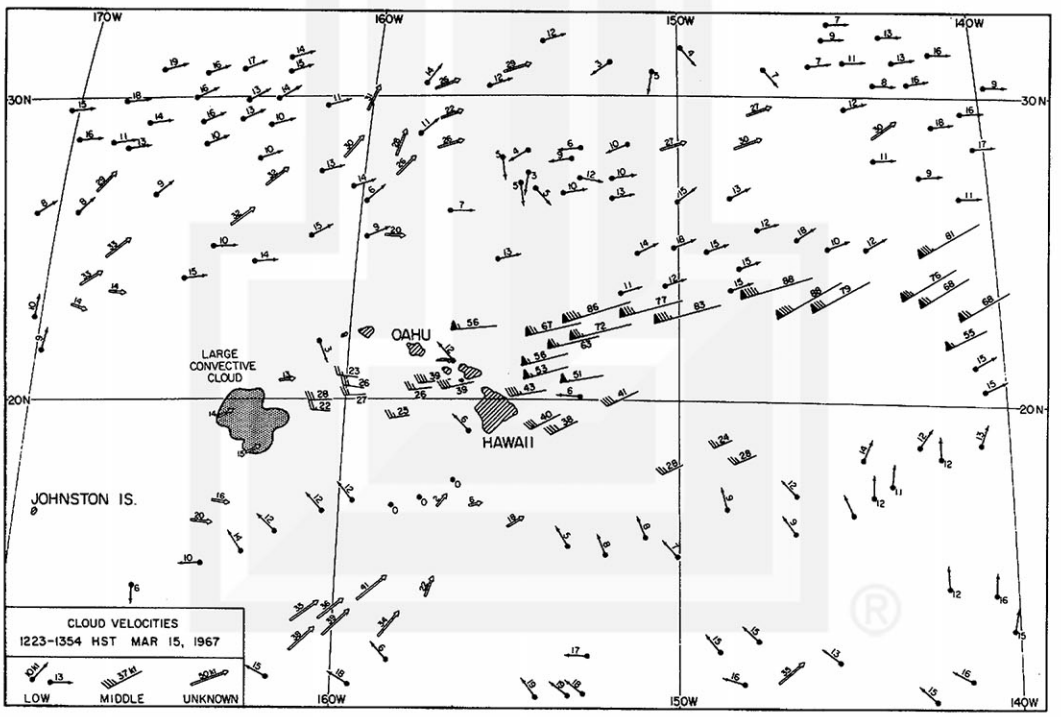

Fig. 6. Computed velocities of all cloud elements shown in Fig. 5. The velocities were computed from the cloud displacements during the period between 1223 and 1354 HST.

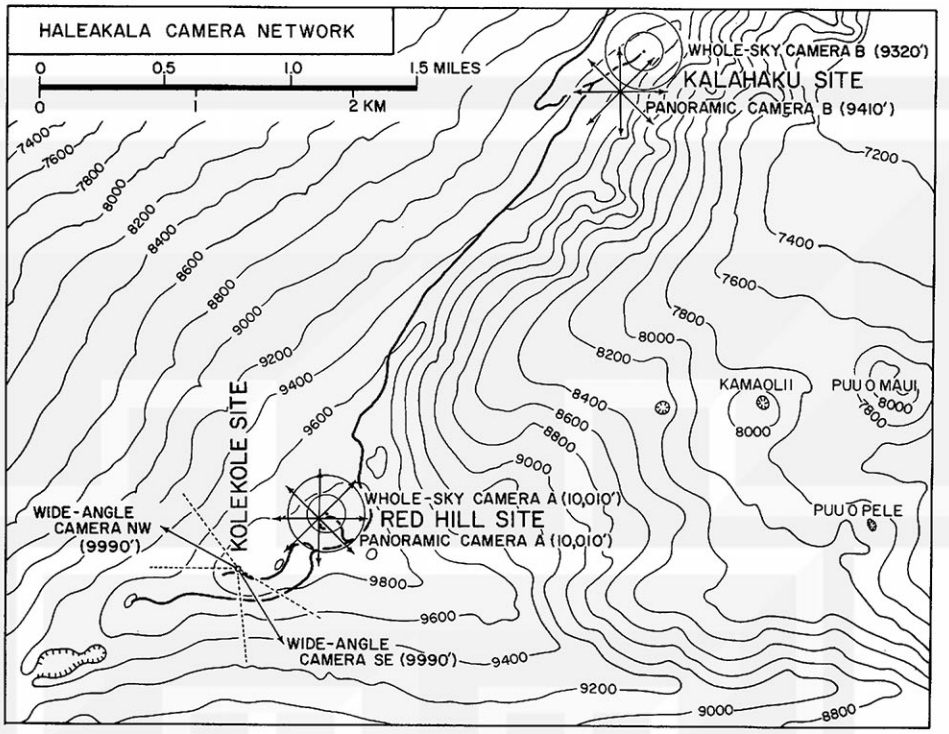

Fig. 7. The Haleakala camera network of March-April 1967. A stereo-pair of whole-sky and panoramic cameras were operated at the Kalahaku site (9320-9410 ft) and the Red Hill Site (10,010 ft) on the north rim of Haleakala volcano on Maui. Two wide-angle time-lapse cameras were operated at the Kolekole site (9990 ft); one to monitor clouds in the direction of the islands of Hawaii and the other in the direction of Lanai.

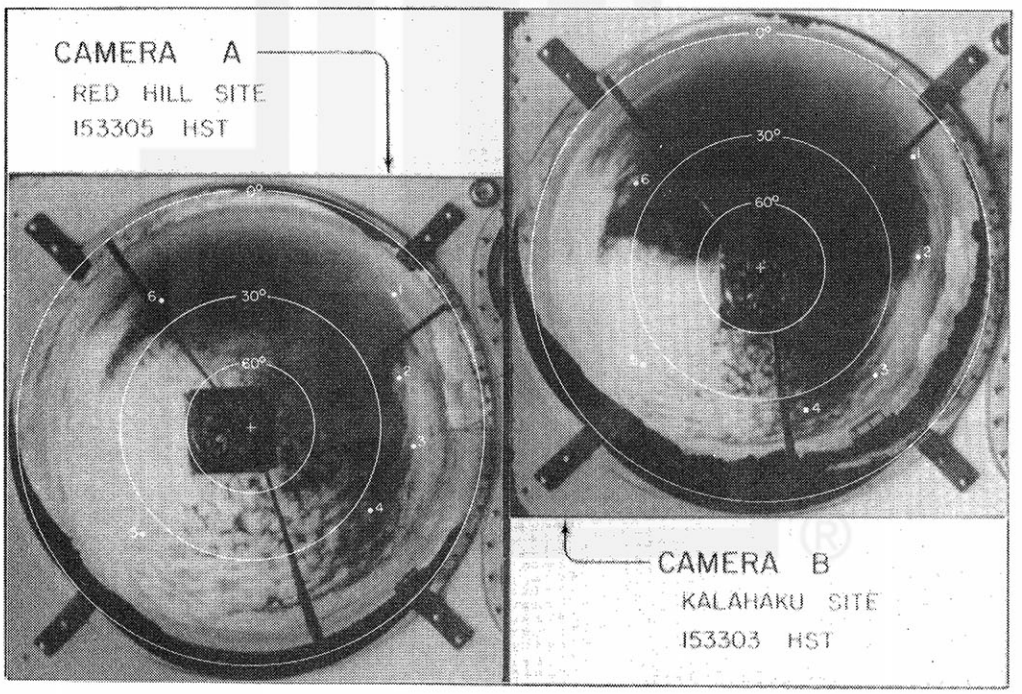

Fig. 8. An example of a stereo-pair of whole-sky pictures taken within 2 sec of each other. The degrees on concentric circles in each picture denote the elevation angles. Selected cloud elements for velocity computation are identified by number 1 through 6.

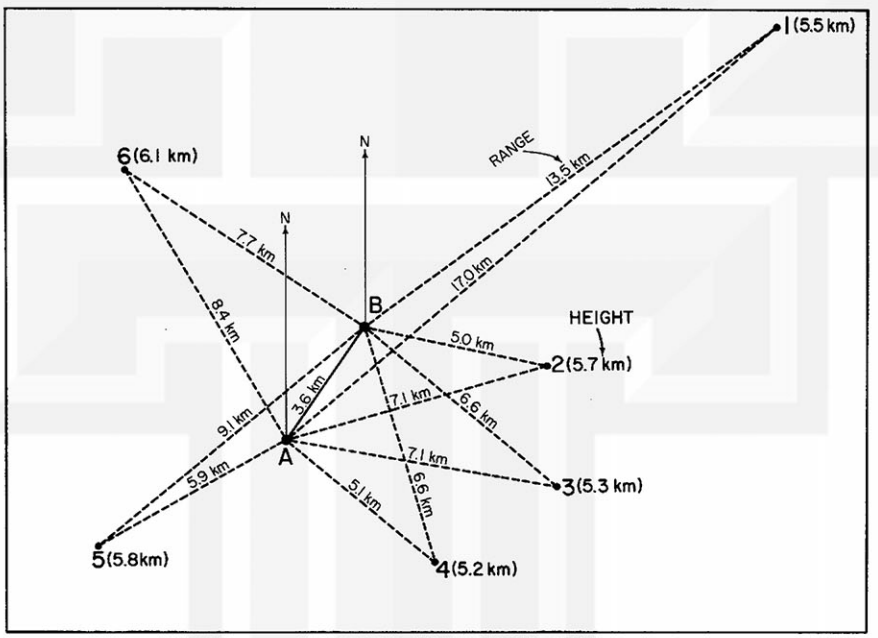

Fig. 9. An example of the plan-position determination by using the pair of pictures shown in Fig. 8. The base line distance was 3.6 km. The height given in parenthesis denotes mean cloud height (MSL) computed from the range and the elevation angles from both sites A and B.

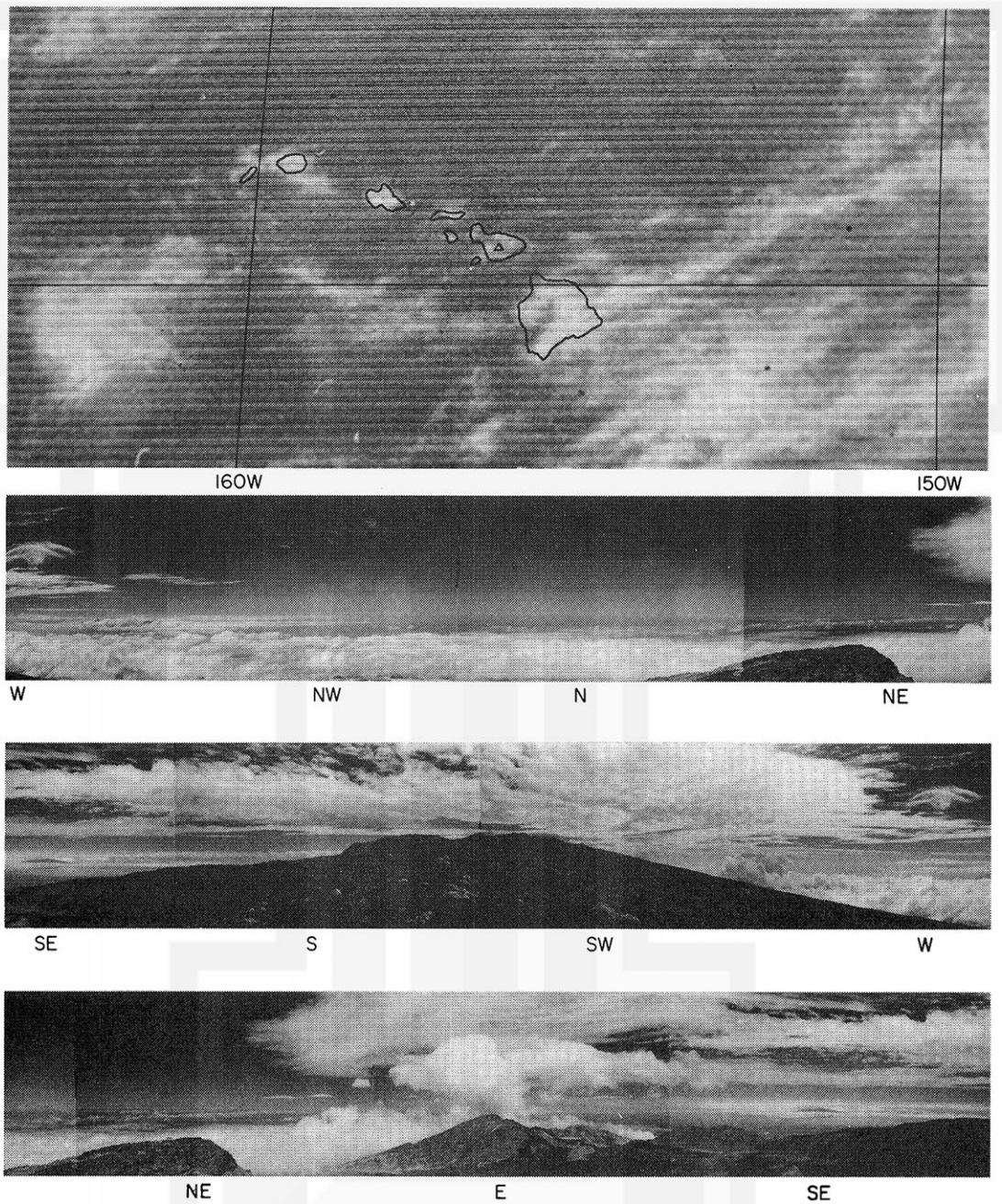

Fig. 10. Comparison of an ATS-I picture started at 1526 HST and a panoramic picture taken at 1520 HST. Boundaries of the islands are added to the ATS-I picture. The Haleakala camera network is shown by a small triangle on Maui. The panoramic view is reproduced in three sections. The apparent horizon is about 200 km which is about the distance to Oahu. The plume-like cloud extending eastward from the large convective cloud appears as altocumulus with practically no vertical development. A standing wave cloud is visible between NE and SE directions.

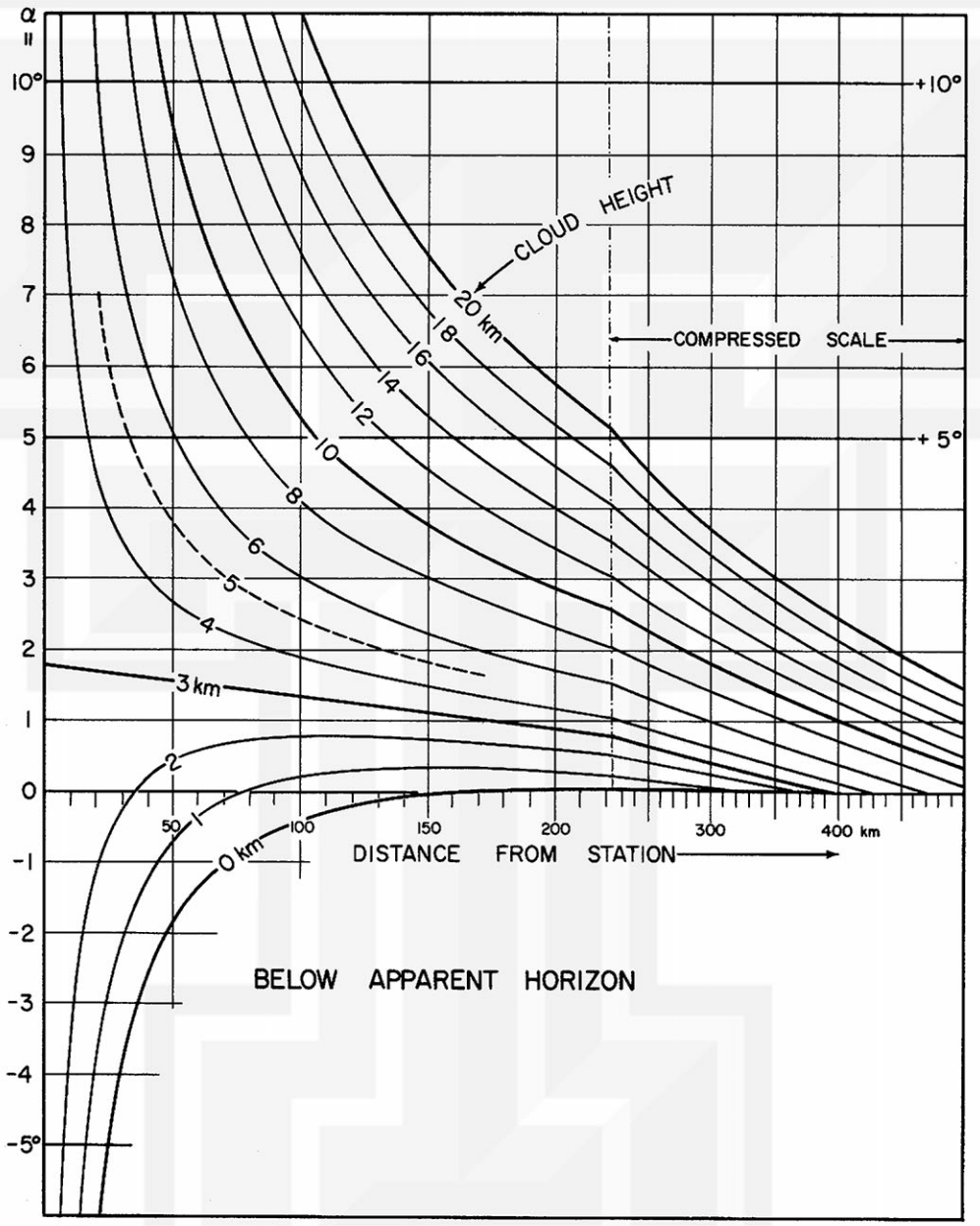

Fig. 11. A nomogram constructed to be used for relating the cloud heights with the distance from Haleakala and the elevation angle measured from the apparent horizon. Note that the horizontal scale was decreased at the range of 250 km. This nomogram can be used to obtain the cloud height from known range and elevation angle. If the height and the elevation angle are known the range can be obtained immediately and verification can be made on the cloud position on an ATS picture. For instance, cirrus at 10 km height will be seen 0.5 deg above the apparent horizon even though its range is as far as 500 km.

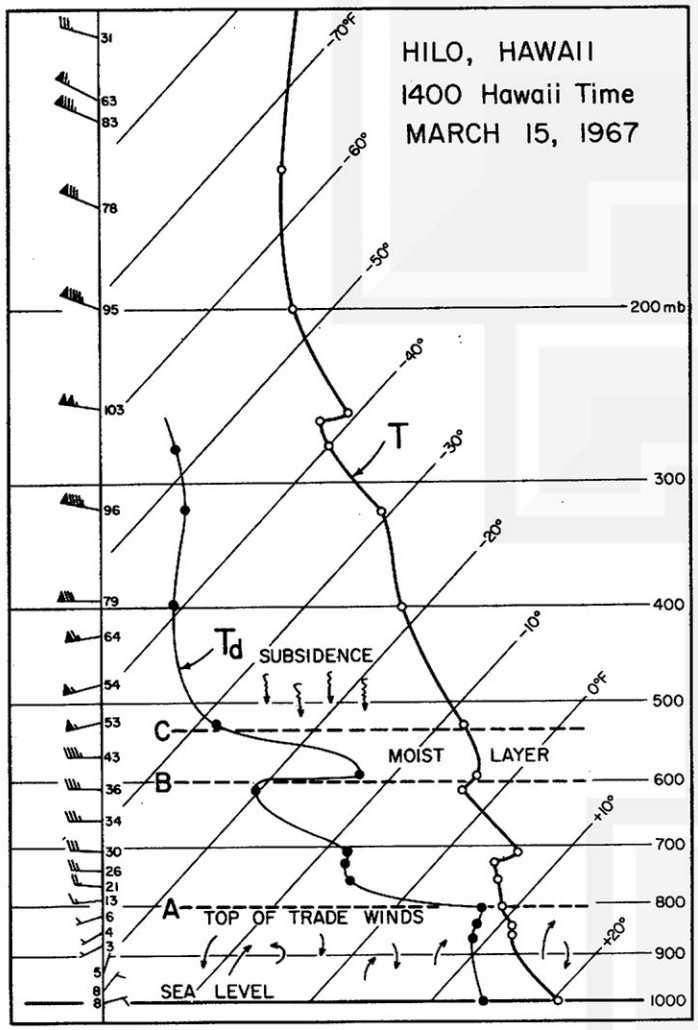

Fig. 12. Sounding from Hilo, Hawaii at 1400 HST 15 March 1967. The moist layer between 600 and 530 mb agrees with the computed height of the altocumulus cloud.

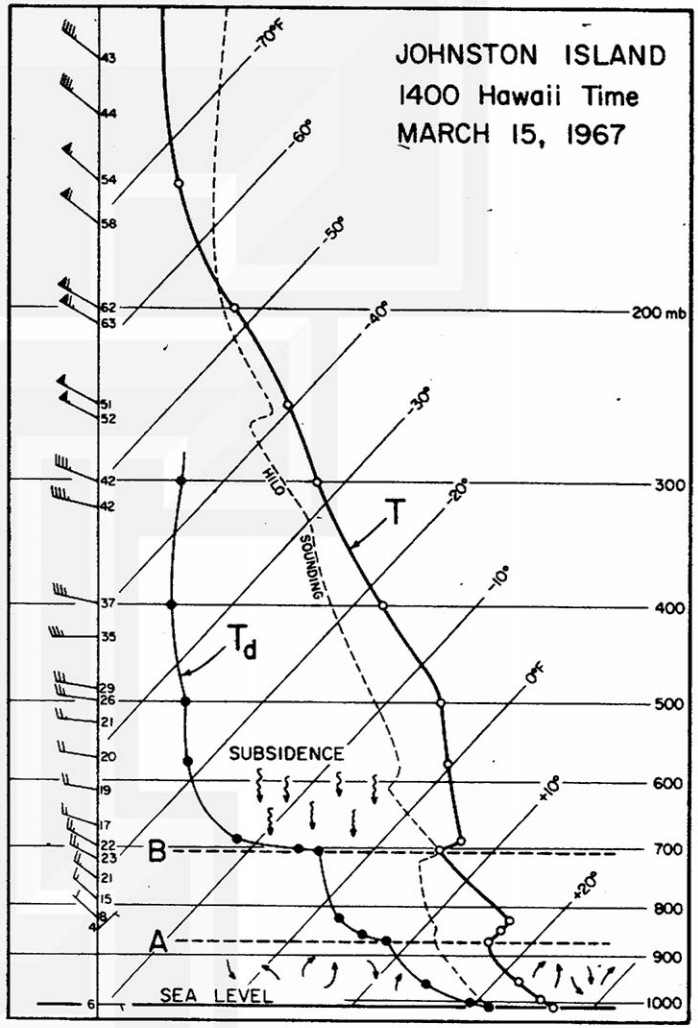

Fig. 13. Sounding from Johnston Island at 1400 HST 15 March 1967.

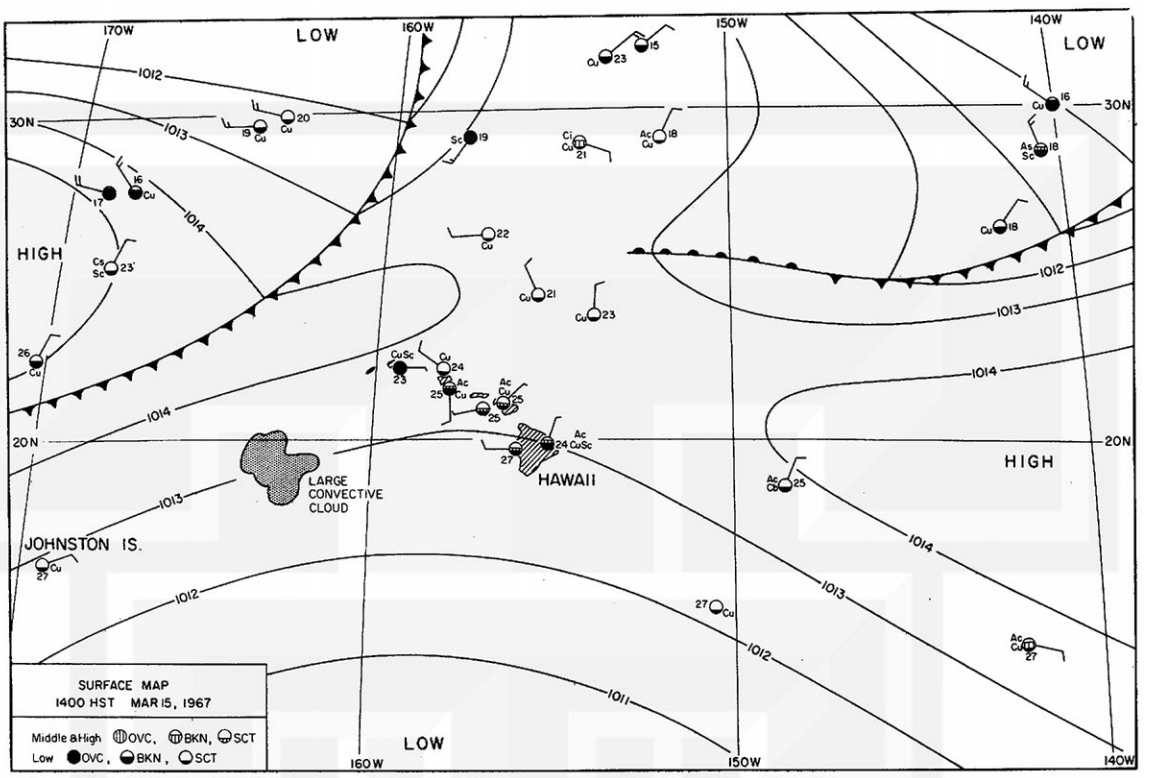

Fig. 14. Surface chart at 1400 HST 15 March 1967 with isobars drawn at 1-mb intervals.

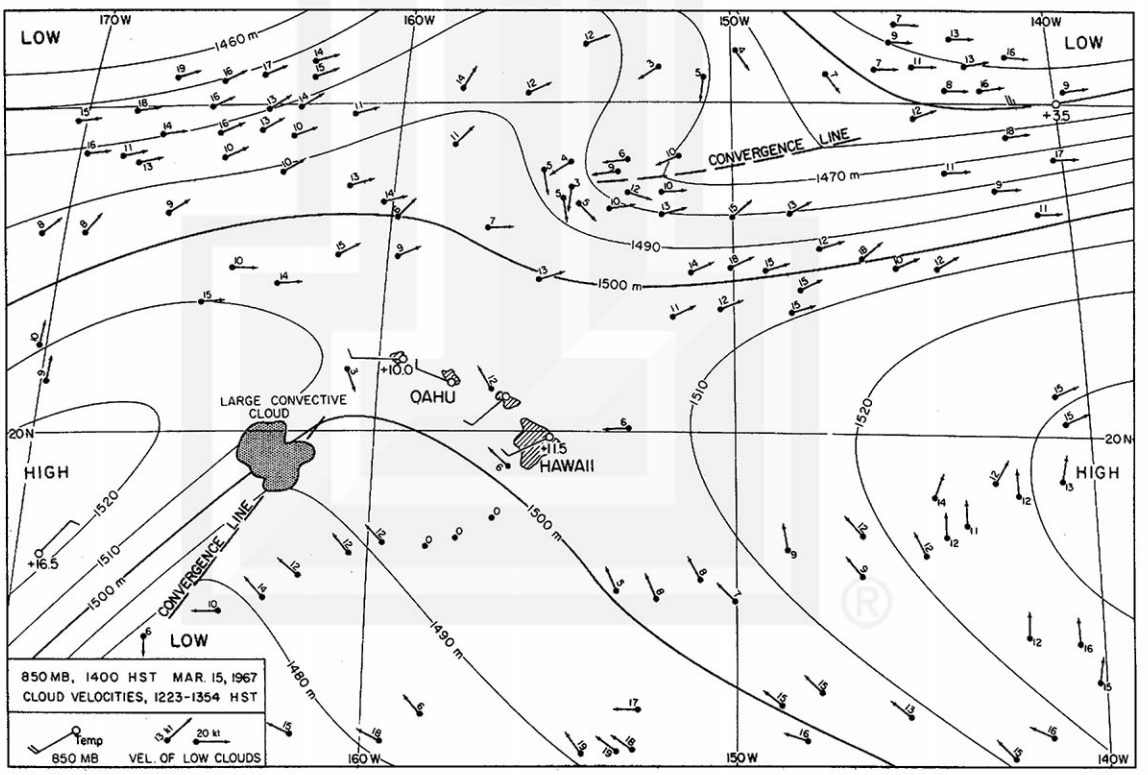

Fig. 15. 850-mb chart with low-cloud velocities. The height contours are drawn for every 10 m. Numbers beside each cloud velocity vector denotes the cloud speed in kt.

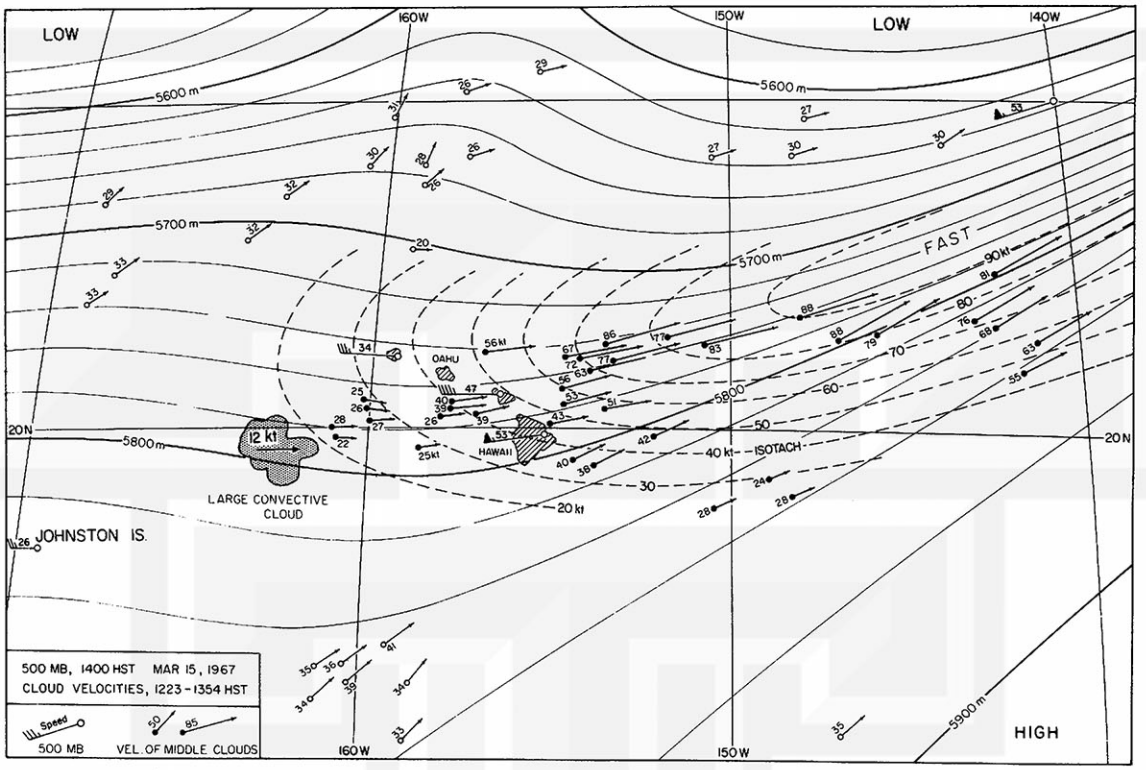

Fig. 16. 500-mb chart with contours drawn for every 20 m. Middle-cloud velocities are plotted and isotachs are drawn for every 10 kt.

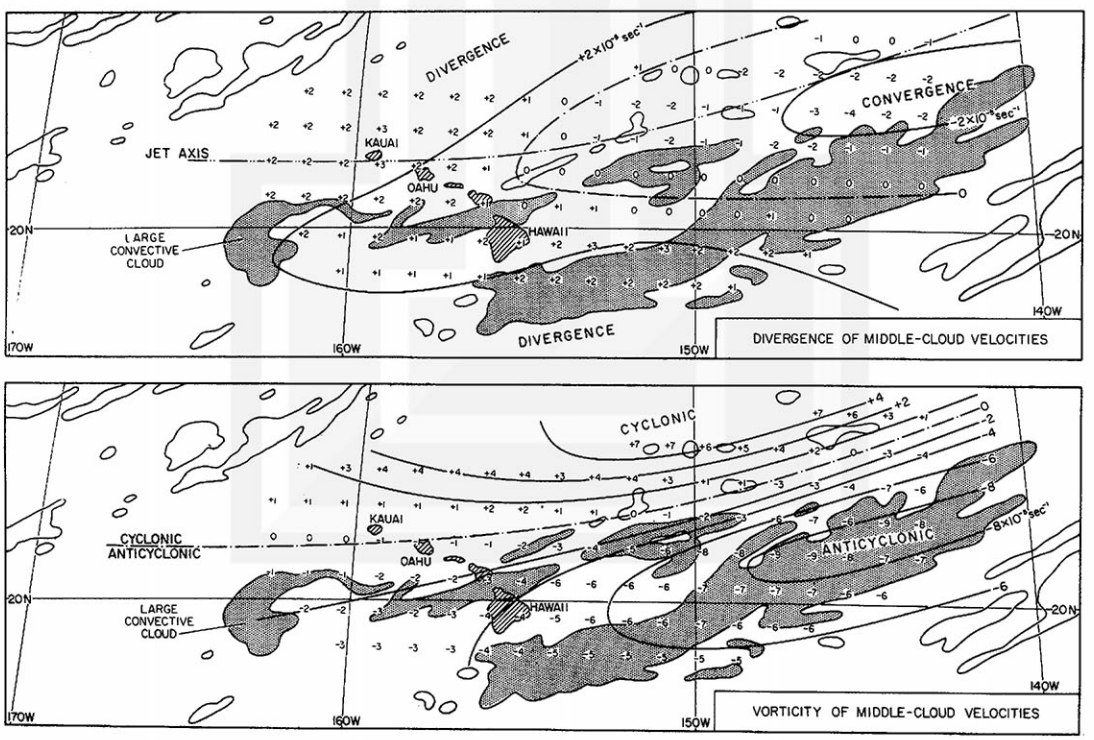

Fig. 17. Divergence and relative vorticity of middle-cloud velocities as shown in Fig. 16. Numbers at grid points are the values in units of 10^{-5} sec^{-1}. Thin irregular lines enclose areas with clouds. Stippled areas denote estimated middle clouds.

MESOMETEOROLOGY PROJECT - - - RESEARCH PAPERS

(Continued from front cover)

42. A Study of Factors Contributing to Dissipation of Energy in a Developing Cumulonimbus - Rodger A. Brown and Tetsuya Fujita
43. A Program for Computer Gridding of Satellite Photographs for Mesoscale Research - William D. Bonner
44. Comparison of Grassland Surface Temperatures Measured by TIROS VII and Airborne Radiometers under Clear Sky and Cirriform Cloud Conditions - Ronald M. Reap
45. Death Valley Temperature Analysis Utilizing Nimbus I Infrared Data and Ground-Based Measurements - Ronald M. Reap and Tetsuya Fujita
46. On the "Thunderstorm-High Controversy" - Rodger A. Brown
47. Application of Precise Fujita Method on Nimbus I Photo Gridding - Lt. Cmd. Ruben Nasta
48. A Proposed Method of Estimating Cloud-top Temperature, Cloud Cover, and Emissivity and Whiteness of Clouds from Short- and Long-wave Radiation Data Obtained by TIROS Scanning Radiometers - T. Fujita and H. Grandoso
49. Aerial Survey of the Palm Sunday Tornadoes of April 11, 1965 - Tetsuya Fujita
50. Early Stage of Tornado Development as Revealed by Satellite Photographs - Tetsuya Fujita
51. Features and Motions of Radar Echoes on Palm Sunday, 1965 - D. L. Bradbury and Tetsuya Fujita
52. Stability and Differential Advection Associated with Tornado Development - Tetsuya Fujita and Dorothy L. Bradbury
53. Estimated Wind Speeds of the Palm Sunday Tornadoes - Tetsuya Fujita
54. On the Determination of Exchange Coefficients: Part II - Rotating and Nonrotating Convective Currents - Rodger A. Brown
55. Satellite Meteorological Study of Evaporation and Cloud Formation over the Western Pacific under the Influence of the Winter Monsoon - K. Tsuchiya and T. Fujita
56. A Proposed Mechanism of Snowstorm Mesojet over Japan under the Influence of the Winter Monsoon - T. Fujita and K. Tsuchiya
57. Some Effects of Lake Michigan upon Squall Lines and Summertime Convection - Walter A. Lyons
58. Angular Dependence of Reflection from Stratiform Clouds as Measured by TIROS IV Scanning Radiometers - A. Rabbe
59. Use of Wet-beam Doppler Winds in the Determination of the Vertical Velocity of Raindrops inside Hurricane Rainbands - T. Fujita, P. Black and A. Loesch
60. A Model of Typhoons Accompanied by Inner and Outer Rainbands - Tetsuya Fujita, Tatsuo Izawa, Kazuo Watanabe, and Ichiro Imai

MESOMETEOROLOGY PROJECT - - - RESEARCH PAPERS

(Continued from inside back cover)

61. Three-Dimensional Growth Characteristics of an Orographic Thunderstorm System - Rodger A. Brown.

62. Split of a Thunderstorm into Anticyclonic and Cyclonic Storms and their Motion as Determined from Numerical Model Experiments - Tetsuya Fujita and Hector Grandoso.

63. Preliminary Investigation of Peripheral Subsidence Associated with Hurricane Outflow - Ronald M. Reap.

64. The Time Change of Cloud Features in Hurricane Anna, 1961, from the Easterly Wave Stage to Hurricane Dissipation - James E. Arnold.

65. Easterly Wave Activity over Africa and in the Atlantic with a Note on the Intertropical Convergence Zone during Early July 1961 - James E. Arnold.

66. Mesoscale Motions in Oceanic Stratus as Revealed by Satellite Data - Walter A. Lyons and Tetsuya Fujita.

67. Mesoscale Aspects of Orographic Influences on Flow and Precipitation Patterns - Tetsuya Fujita.

68. A Mesometeorological Study of a Miniphoon - Hidetoshi Arakawa, Kazuo Watanabe, Kiyoshi Tsuchiya and Tetsuya Fujita.

69. Estimation of Tornado Wind Speed from Characteristic Ground Marks - Tetsuya Fujita, Dorothy L. Bradbury, and Peter G. Black.

70. Computation of Height and Velocity of Clouds from Dual, Whole-Sky, Time-Lapse Picture Sequences - Dorothy L. Bradbury and Tetsuya Fujita